A Theory for the Indian Ocean Dipole–Zonal Mode*

TIM LI AND BIN WANG

International Pacific Research Center, University of Hawaii at Manoa, Honolulu, Hawaii

C.-P. CHANG

Department of Meteorology, Naval Postgraduate School, Monterey, California

YONGSHENG ZHANG

International Pacific Research Center, University of Hawaii at Manoa, Honolulu, Hawaii

(Manuscript received 12 June 2002, in final form 20 March 2003)

ABSTRACT

Four fundamental differences of air–sea interactions between the tropical Pacific and Indian Oceans are identified based on observational analyses and physical reasoning. The first difference is represented by the strong contrast of a zonal cloud–SST phase relationship between the warm and cool oceans. The in-phase cloud–SST relationship in the warm oceans leads to a strong negative feedback, while a significant phase difference in the cold tongue leads to a much weaker thermodynamic damping. The second difference arises from the reversal of the basic-state zonal wind and the tilting of the ocean thermocline, which leads to distinctive effects of ocean waves. The third difference lies in the existence of the Asian monsoon and its interaction with the adjacent oceans. The fourth difference is that the southeast Indian Ocean is a region where a positive atmosphere–ocean thermodynamic feedback exists in boreal summer.

A conceptual coupled atmosphere–ocean model was constructed aimed to understand the origin of the Indian Ocean dipole–zonal mode (IODM). In the model, various positive and negative air–sea feedback processes were considered. Among them were the cloud–radiation–SST feedback, the evaporation–SST–wind feedback, the thermocline–SST feedback, and the monsoon–ocean feedback. Numerical results indicate that the IODM is a dynamically coupled atmosphere–ocean mode whose instability depends on the annual cycle of the basic state. It tends to develop rapidly in boreal summer but decay in boreal winter. As a result, the IODM has a distinctive evolution characteristic compared to the El Niño. Sensitivity experiments suggest that the IODM is a weakly damped oscillator in the absence of external forcing, owing to a strong negative cloud–SST feedback and a deep mean thermocline in the equatorial Indian Ocean.

A thermodynamic air–sea (TAS) feedback arises from the interaction between an anomalous atmospheric anticyclone and a cold SST anomaly (SSTA) off Sumatra. Because of its dependence on the basic-state wind, the nature of this TAS feedback is season dependent. A positive feedback occurs only in northern summer when the southeasterly flow is pronounced. It becomes a negative feedback in northern winter when the northwesterly wind is pronounced. The phase locking of the IODM can be, to a large extent, explained by this seasonal-dependent TAS feedback. The biennial tendency of the IODM is attributed to the monsoon–ocean feedback and the remote El Niño forcing that has a quasi-biennial component.

In the presence of realistic Niño-3 SSTA forcing, the model is capable of simulating IODM events during the last 50 yr that are associated with the El Niño, indicating that ENSO is one of triggering mechanisms. The failure of simulation of the 1961 and 1994 events suggests that other types of climate forcings in addition to the ENSO must play a role in triggering an IODM event.

1. Introduction

This study is motivated by the observational discovery that there is a remarkable SST dipole (or zonal) mode in the equatorial Indian Ocean (IODM) and by the hypothesis that this zonal SST mode may arise from dynamic atmosphere–ocean interactions in the Indian Ocean (IO; Saji et al. 1999; Webster et al. 1999). Although similar dipole events with weaker amplitudes have been noticed previously (e.g., Hackert and Hastenrath 1986; Reverdin et al. 1986), the 1997 IODM event attracted great public attention when it reached high magnitude and was associated with severe floods in eastern Africa and droughts over Indonesia. It has been suggested that the unusual Indian monsoon–El Niño–Southern Oscillation (ENSO) relationship in 1997

* School of Ocean and Earth Science and Technology Contribution Number 6172, and International Pacific Research Center Contribution Number 203.

Corresponding author address: Prof. Tim Li, IPRC, and Dept. of Meteorology, University of Hawaii at Manoa, 2525 Correa Rd., Honolulu, HI 96822.
E-mail: timli@hawaii.edu

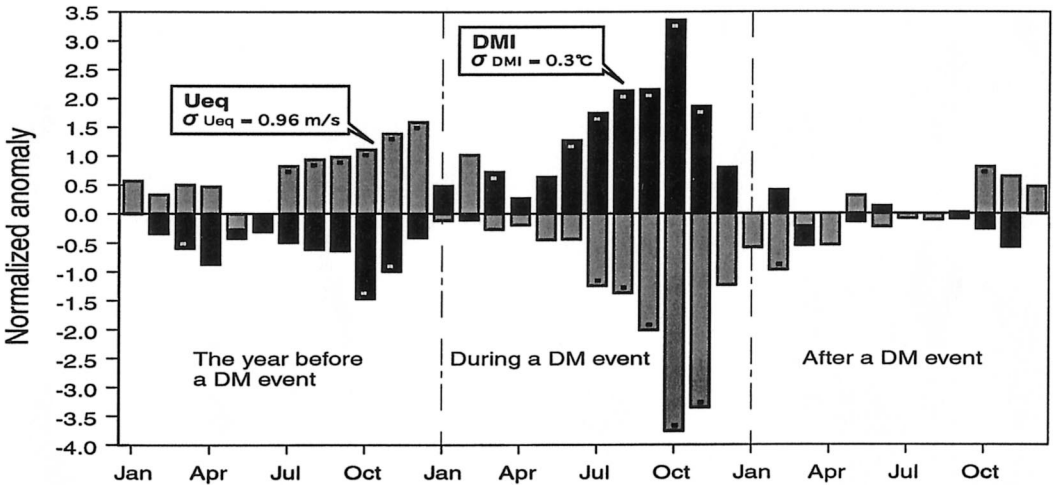

FIG. 1. Time evolution of the dipole mode index defined as the SSTA difference between the western and eastern Indian Ocean (dark-shaded bar) and the zonal wind anomaly (light-shaded bar), adopted from Saji et al. (1999).

may result from this abnormal SST condition in the IO (Ashok et al. 2001).

Figure 1 illustrates the evolution of composite SST and zonal wind anomalies associated with the IODM. A remarkable feature inferred from this figure is the close zonal wind–SST relationship, indicating a strong air–sea coupling over the IO. In fact this has prompted some investigators (e.g., Chamber et al. 1999) to hypothesize that the same mechanism as that in ENSO might work in the IO. On the other hand, it is noted that the tropical Pacific and IO have remarkable differences in the basic-state wind and SST fields. A theoretical study by Wang and Xie (1998) pointed out that ocean–atmosphere interactions have distinctive characters in the warm pool and cold tongue. This motivates the first scientific question; namely, what are fundamental differences of air–sea interaction processes between the tropical Pacific and Indian Oceans? Another feature from Fig. 1 is that the IODM develops rapidly in boreal summer and reaches its mature phase in October. This temporal evolution characteristic differs remarkably from the El Niño cycle, which has a peak phase in northern winter. Thus, the second fundamental question we address is what causes the phase locking of the IODM. The third feature inferred from Fig. 1 is that the IODM tends to have a biennial tendency, that is, the zonal wind and SST gradient anomalies change the sign from one year to the following year. What is the physical mechanism responsible for this biennial tendency?

In this study we intend to address these questions. Our strategy is first to analyze the differences of air–sea coupling processes between the tropical Pacific and Indian Oceans based on observational analyses and physical reasoning (section 2). Then based on these analyses we build a conceptual coupled model in an attempt to understand the mechanism for the IODM (section 3). The model solution in the absence of any external forcing is discussed in section 4. In section 5 we examine the role of ENSO and intraseasonal oscillation (ISO) forcing. In subsequent sections we further discuss the processes that lead to the phase-locking and biennial tendency of the IODM and the effect of ocean waves. A concluding remark and discussions are given in the last section.

2. Fundamental differences of air–sea interactions between the tropical Pacific and IO

In this section, by use of observational analyses and physical reasoning, we intend to demonstrate that there are four fundamental differences of air–sea interaction processes between the tropical Pacific and Indian Oceans.

The first difference lies in the zonal phase relationship between the anomalous cloud and SST. Figure 2 shows the observed SST and net surface shortwave radiation fields obtained from the El Niño and IODM composites, respectively, for a period of 1950–98. [For the El Niño composites, 12 El Niño episodes were selected, whereas for the IODM composite, six dipole events were selected following Saji et al. (1999).] A remarkable difference between the two composites is that the SST and shortwave radiation (or cloud) anomalies have significant zonal phase differences in the eastern Pacific but not in the IO. The differences arise from the distinctive atmospheric responses to an SST anomaly (SSTA) in the warm pool and cold tongue. In general, atmospheric deep convection is triggered in the region where SST exceeds 27.5°C. This is why convection associated with El Niño is often observed in the central equatorial Pacific even though the maximum SSTA appears in the eastern Pacific. Because of this phase difference, the reduction of the downward shortwave radiation due to

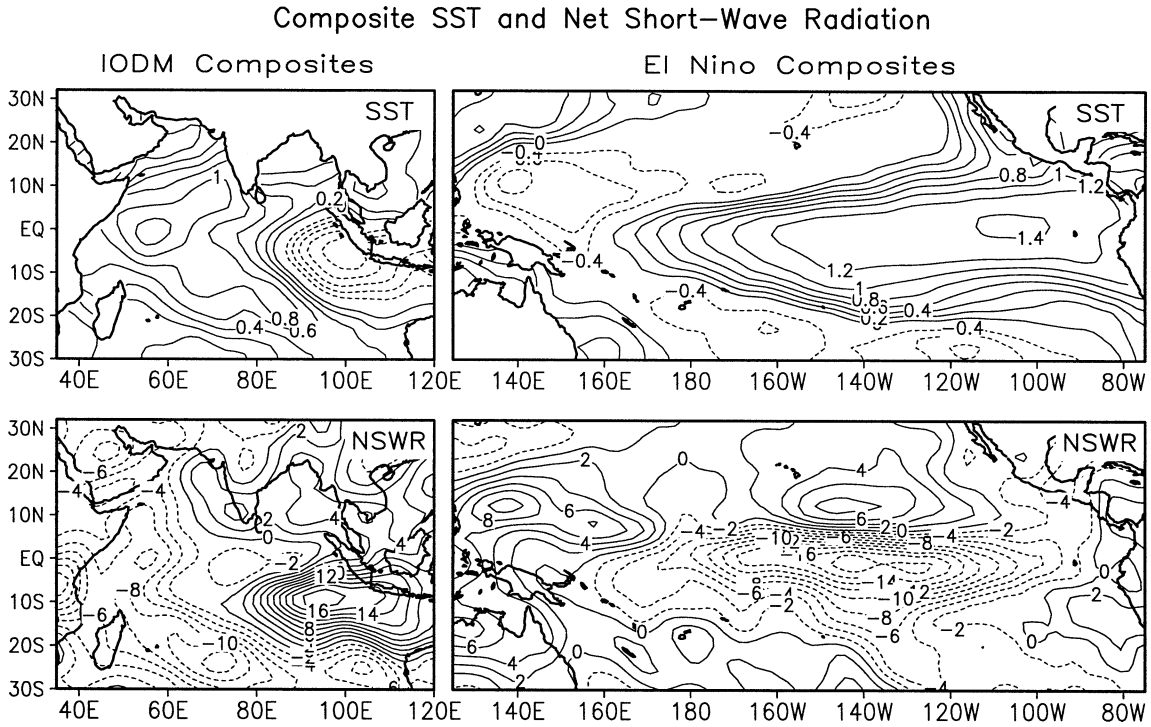

FIG. 2. Horizontal structure of SSTA (°C) and net shortwave radiation anomalies (W m^{-2}) composed from 12 major El Niño and six IODM events during 1950–99.

the deep convection cannot efficiently damp the El Niño. In warm oceans, on the other hand, a modest SSTA may induce deep convection in situ, so that the anomalous SST and clouds are generally in phase. The increased clouds tend to reduce the downward shortwave radiation and thus decrease the SST, leading to a negative feedback between the atmosphere and ocean.

The strength of the negative cloud–radiation–SST feedback in the warm ocean may be estimated based on a linear Newtonian damping formula:

$$D_{\mathrm{SW}}T = -\frac{Q_{\mathrm{SW}}}{\rho c_w h},$$

where D_{SW} is the Newtonian cooling coefficient representing the strength of the negative feedback, Q_{SW} is net downward shortwave radiation, T is SST, ρ and c_w are water density and specific heat, and h is the mean depth of the oceanic mixed layer. According to the composite SST–radiation relationship in the IO (Fig. 2), a negative SSTA of -1.0°C corresponds to a net shortwave radiation anomaly of 20 W m^{-2}. Thus, for a mixed layer depth of 50 m, one may calculate D_{SW}, which corresponds to a reversed damping timescale of 100 days. Such a strong thermodynamic damping implies that SST variability in the tropical IO is in general small except in regions where there exists a strong positive feedback (that overcomes the negative feedback) and/or there is strong, persistent external forcing.

The second difference is attributed to the great contrast of the basic-state zonal wind and the effect of ocean waves. Whereas the tropical Pacific is dominated by easterly trades, the winds in the tropical IO are characterized by cross-equatorial monsoonal circulation. At the equator, the annual mean wind is easterly in the Pacific but weaker westerly in the IO. Such a difference results in opposite thermocline gradients across the two ocean basins (Fig. 3).

The reversal of the basic-state wind and zonal thermocline gradient in the IO implies that the effect of equatorial ocean waves might differ from the Pacific counterpart. The schematic diagram of Fig. 4 illustrates how the wave effect could be different. In the Pacific, an El Niño warming leads to westerly anomalies in the central equatorial Pacific that further induce oceanic Rossby waves with negative thermocline depth anomalies. After reflected in the western boundary, the Rossby waves become upwelling Kelvin waves that propagate eastward, reversing the sign of the SSTA later (Schopf and Suarez 1988; Battisti and Hirst 1989). Thus, in the El Niño scenario, ocean waves act as a negative feedback agent and are responsible for the phase reversal. There is an energy loss in the wave reflection process. In the El Niño scenario this energy loss is compensated by the very shallow thermocline in the eastern Pacific so that the weakened, reflected waves can still make significant SST changes. Unlike the Pacific where thermocline is tilted to the east, the thermocline in the equatorial IO is shallower toward the west. As a result,

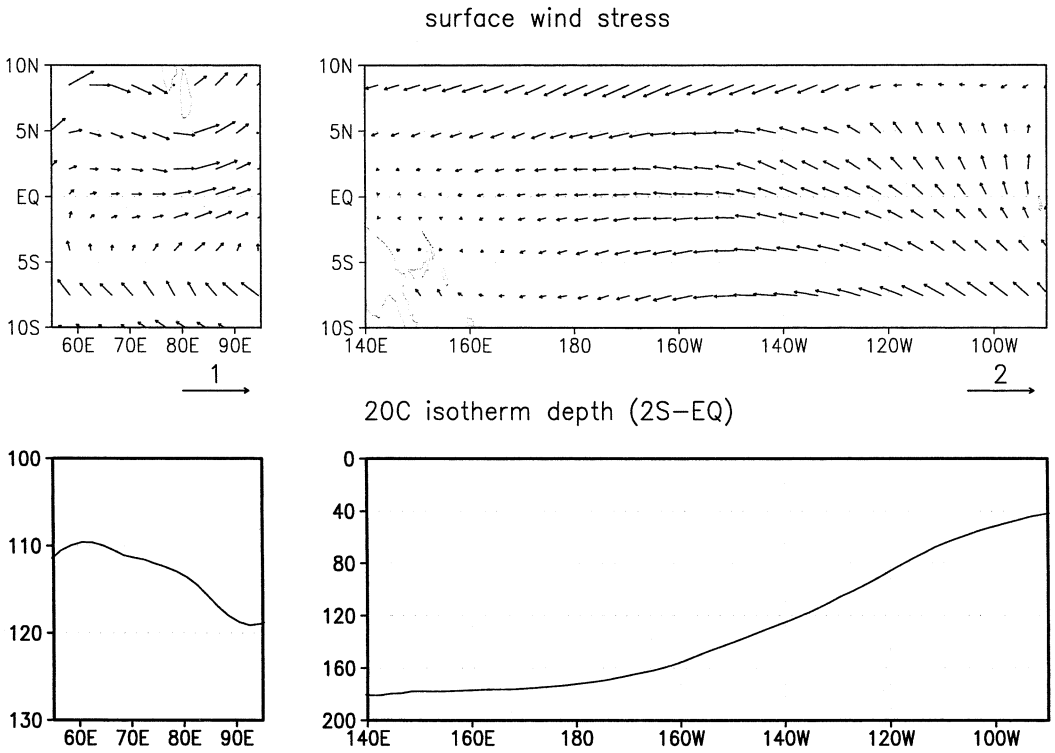

FIG. 3. Structure of observed annual mean surface wind stress (N m^{-2}) fields and zonal distribution of the ocean 20°C isotherm depth (m) fields along the equatorial Pacific and Indian Ocean.

except a few hundred kilometers off the coast of Sumatra, the SST is more sensitive to the wave-induced thermocline change in the west than in the east. In the IODM scenario oceanic Rossby waves generated by the curl of anomalous wind stress in response to a positive phase of the IODM[1] carry deeper thermocline signals and propagate westward, enhancing the warm SSTA in the western IO where the mean thermocline is relatively shallow. As a result, the ocean waves have a positive effect on the IODM during the initial development stage. The reflected Kelvin waves also have a negative effect on the SSTA in the eastern IO, but this effect is overwhelmed by a positive thermodynamic air–sea feedback off Sumatra in summer (see discussion below). As a result, the negative wave effect was realized only in the late development stage when it contributed to a conversion from a dipole mode to a basin mode (see discussions in section 7). The signals of the Rossby wave propagation and associated ocean warming were clearly detected by satellite observations (e.g., Webster et al. 1999; Ueda and Matsumoto 2000) and well simulated by oceanic models (e.g., Murtugudde et al. 2000; Li et al. 2002).

The third difference lies in the existence of the South Asian monsoon and its interaction with adjacent oceans. A warm SSTA in the IO may enhance the Indian monsoon through increased moisture fluxes (Meehl 1997). An enhanced monsoon may further affect the equatorial IO through remote and local processes (Chang and Li 2000, hereafter CL00). To investigate the possible impact of the IODM on the Indian monsoon, we conducted 10 ensemble atmospheric general circulation model (AGCM) experiments with the Max Planck Institute for Meteorology ECHAM4 model in a T42L19 resolution. For each ensemble run, a slightly different initial condition was used. The AGCM was forced by observed monthly SST fields in 1997 in the tropical IO (30°S–30°N, 40°–110°E) and climatological SST fields elsewhere. The atmospheric response to the IODM was obtained by subtracting the ensemble mean fields from those in a control experiment in which the climatological monthly SST fields were specified in global oceans. The AGCM ensemble simulations indicate that a positive phase of the IODM tends to enhance the Indian monsoon rainfall, which is consistent with results from a different AGCM by Ashok et al. (2001).

How does the anomalous monsoon further feed back to the IODM? We argue that a strong Indian monsoon may enhance the northward cross-equatorial wind along the coast of Africa and cyclonic monsoon westerly near the equatorial central IO, leading to a cold SSTA in the western IO (through enhanced surface evaporation, ocean mixing, and coastal upwelling) and a warm SSTA

[1] A positive phase denotes a positive (negative) SSTA in the western (eastern) Indian Ocean, following Saji et al. (1999).

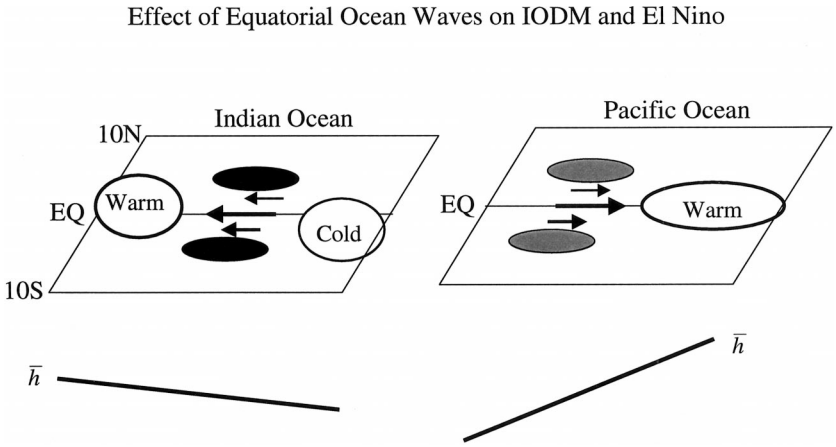

FIG. 4. Schematic diagram of effect of equatorial oceanic waves on the El Niño and the IODM. Dark- (light-) shaded regions represent positive (negative) ocean thermocline depth anomalies.

in the eastern IO. Meanwhile, the strengthened monsoon may enhance the large-scale east–west circulation and leads to a positive SSTA in the western Pacific/Maritime Continent (CL00). As a result, the local Walker cell over the IO is enhanced. The enhanced Walker cell favors a warm (cold) SSTA in the eastern (western) IO through induced anomalous downwelling (upwelling) and the change of the thermocline depth/subsurface temperature. Both the remote and local processes tend to damp the original IODM. Therefore, in addition to the cloud–radiation–SST feedback, the monsoon may exert another type of negative feedback on the IODM. The argument above is supported by coupled model simulations (Lau and Nath 2003a) that a weakened Indian monsoon due to El Niño forcing leads to weakened along-coastal winds and surface warming off Africa and a cold SSTA off Sumatra.

The fourth difference is the occurrence of a positive thermodynamic air–sea (TAS) feedback in the southeast IO in northern summer. Figure 5 is a schematic diagram illustrating how this positive feedback works. Compared to the southeast coasts of the tropical Pacific and Atlantic Oceans characterized by cold SST tongues and low stratus clouds, the southeast IO (off Sumatra) is a region with persistent high mean SST and deep convection. Assume initially there is a modest cold SSTA off Sumatra. Since the southeast IO is a region of intense convection, the cold SSTA implies the decrease of atmospheric convective heating or an atmospheric heat sink. According to Gill's (1980) solution, the heat sink will induce a descending Rossby wave response to its west, resulting in an anomalous low-level anticyclonic flow. In northern summer the mean flow is southeasterly. Thus the anomalous wind enhances the total wind speed and lowers the SST further through enhanced surface evaporation, vertical mixing and coastal upwelling.

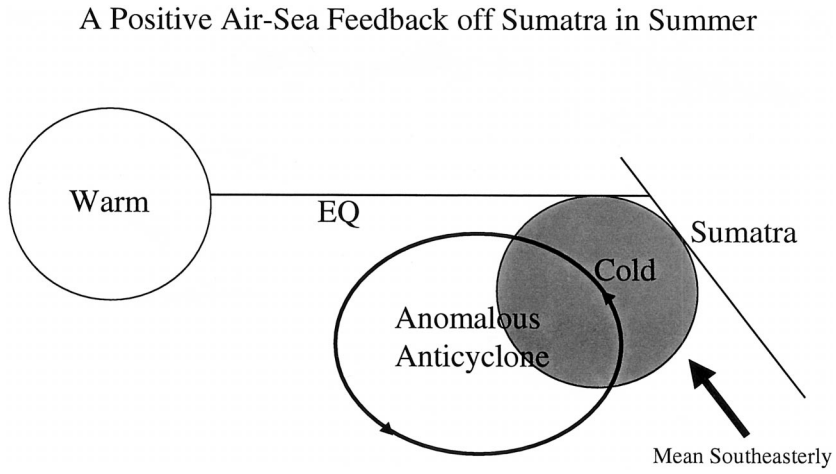

FIG. 5. Schematic diagram illustrating a positive thermodynamic air–sea feedback between an anomalous atmospheric anticyclone and a cold SSTA off Sumatra in the presence of the boreal summer mean southeasterly flow.

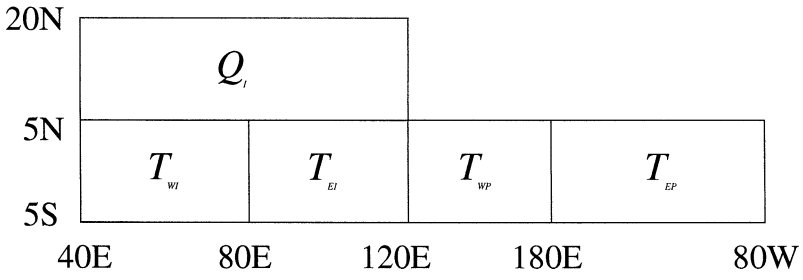

FIG. 6. Schematics of the five-box model. See text for details.

Through this positive air–sea feedback, the cold SSTA and the anomalous anticyclone develop. A similar feedback mechanism has been discussed previously by Wang et al. (2000) with regard to air–sea interactions in the western North Pacific.

Because of its dependence on the basic-state wind, the nature of this TAS feedback is season dependent (see discussions in Wang et al. 2003). The positive feedback is only efficient in boreal summer when the southeasterly flow is pronounced. With the seasonal change of the background flows from southeasterly in boreal summer to northwesterly in boreal winter, the same anomalous wind tends to reduce the total wind speed and thus damp the original cold SSTA. Thus, this mechanism reflects a negative feedback in northern winter. Because of its strong seasonal dependence, this TAS feedback mechanism explains the rapid development of the IODM in boreal summer and its mature phase in fall.

How does the size of the IO basin matter? First, it may directly impact the basic-state fields. Second, the change of the basin size may modulate the strength of various aforementioned air–sea feedbacks. For instance, the monsoon–ocean feedback might become weaker if the IO basin were twice as large. The change of the basin size will certainly influence the travel time of the ocean waves, and may also affect the remote El Niño forcing effect. Given that the essential factor for the TAS and cloud–SST feedbacks lies in the existence of the warm pool, the two feedback processes may still work even if the IO basin were extended westward to cover Africa and the Atlantic Ocean.

3. A conceptual coupled model for the IODM

a. Governing equations

Our strategy is to construct the simplest model possible while considering essential air–sea feedback processes in the IO. For this purpose, we constructed a five-box model illustrated in Fig. 6. Along the equator, the Indian Ocean is divided into two equal volume boxes, with T_{WI} and T_{EI} representing, respectively, the SSTA in the western IO (40°–80°E) and eastern IO (80°–120°E). To consider the monsoon–ocean interaction and the remote ENSO forcing, we consider additional three boxes. They represent, respectively, the South Asian monsoon region, the equatorial western Pacific/maritime continent (120°E–180°), and the eastern equatorial Pacific (180°–80°W). The time change rate of the SSTA in the western equatorial IO may be written as

$$\frac{dT_{\mathrm{WI}}}{dt} = -\lambda\Delta\overline{q}_{\mathrm{WI}}\frac{\overline{V}_{\mathrm{WI}}V_{\mathrm{WI}}}{V_0} - (\lambda V_0\kappa + D_{\mathrm{SW}})T_{\mathrm{WI}} - u_I\overline{T}_I^{(x)} - \overline{u}_I T_I^{(x)} - w_{\mathrm{WI}}\overline{T}_{\mathrm{WI}}^{(z)} - \frac{\overline{w}_{\mathrm{WI}}}{h}(T_{\mathrm{WI}} - \gamma\eta_{\mathrm{WI}}), \quad (1)$$

where the first two terms in the right-hand side of (1) represent linearized surface latent heat flux anomalies associated with the along-coastal wind and air–sea specific humidity difference; the third term, the cloud–radiation–SST feedback; the fourth and fifth terms, horizontal advection; and the last three terms, the vertical temperature advection associated with anomalous upwelling and thermocline displacement. In (1), V, u, w, and η denote, respectively, the along-coastal wind, ocean zonal current, vertical velocity at the base of the oceanic mixed layer, and the thermocline depth; Δq denotes the air–sea specific humidity difference; γ represents the strength of subsurface ocean temperature variations associated with the thermocline displacement; $T^{(x)}$ and $T^{(z)}$ denote the zonal and vertical ocean temperature gradients; and h represents the depth of the mixed layer. Subscript WI stands for the western IO. Variables with (without) an overbar represent the basic-state (anomaly) fields; V_0 denotes a constant surface wind speed; κ an empirical constant relating SST and specific humidity; and $\lambda = \rho_a c_D L/\rho c_w h$, where ρ and ρ_a are the density of water and surface air, c_w the specific heat of water, c_D the drag coefficient, and L the latent heat.

Similarly, the time change rates of the SSTA in the eastern equatorial IO and the western Pacific are governed by

$$\frac{dT_{\mathrm{EI}}}{dt} = -\lambda\Delta\overline{q}_{\mathrm{EI}}\frac{\overline{V}_{\mathrm{EI}}V_{\mathrm{EI}}}{V_0} - (\lambda V_0\kappa + D_{\mathrm{SW}})T_{\mathrm{EI}} - \overline{u}_I T_I^{(x)} - u_I\overline{T}_I^{(x)} - w_{\mathrm{EI}}\overline{T}_{\mathrm{EI}}^{(z)} - \frac{\overline{w}_{\mathrm{EI}}}{h}(T_{\mathrm{EI}} - \gamma\eta_{\mathrm{EI}}), \quad (2)$$

$$\frac{dT_{\mathrm{WP}}}{dt} = -\lambda\Delta\overline{q}_{\mathrm{WP}}\frac{\overline{U}_{\mathrm{WP}}U_{\mathrm{WP}}}{V_0} - (\lambda V_0\kappa + D_{\mathrm{SW}})T_{\mathrm{WP}} - u_{\mathrm{CP}}\overline{T}^{(x)}_{\mathrm{CP}} - \overline{u}_{\mathrm{CP}}T^{(x)}_{\mathrm{CP}} - w_{\mathrm{WP}}\overline{T}^{(z)}_{\mathrm{WP}} - \frac{\overline{w}_{\mathrm{WP}}}{h}(T_{\mathrm{WP}} - \gamma\eta_{\mathrm{WP}}), \quad (3)$$

where subscripts EI, WP, and CP denote the eastern IO, western, and central equatorial Pacific, respectively; and U denotes the zonal wind component. Although the SST equations look similar in the western and eastern IO, the processes that cause the SST change in the two regions may differ significantly. Murtugudde et al. (2000) showed that the along-coastal wind was essential to initiate an SSTA off Sumatra. A mixed-layer heat budget analysis indicated that the latent heat flux and vertical advection primarily determined the SSTA in the east pole, while in the west pole it was caused by 3D temperature advection (Li et al. 2002). The thermocline displacement was found to be important in the southwest IO, where a minimum center appeared in the annual-mean thermocline depth field (Xie et al. 2002).

The change of the thermocline depth in the western and eastern IO in the model depends on following two processes: 1) a fast response to the wind forcing in the central equatorial IO so that the thermocline depth and zonal wind anomalies are in a Sverdrup balance (Neelin 1991; Li 1997), and 2) a slow adjustment owing to the propagation of ocean waves (Schopf and Sureaz 1988):

$$\eta_{\mathrm{WI}} = -\frac{\rho_a c_D V_0 L_I}{2g'\rho H}U_I(t) - c_0 U_I(t - \tau_1), \quad (4a)$$

$$\eta_{\mathrm{EI}} = \frac{\rho_a c_D V_0 L_I}{2g'\rho H}U_I(t) - c_0 U_I(t - \tau_1 - \tau_2), \quad (4b)$$

where g' is the reduced gravity; H the mean depth of the ocean thermocline; L_I the half-width of the equatorial IO basin; $\alpha = \rho_a c_D V_0$, $\tau_1 = L_I/C_R$, and $\tau_2 = 2L_I/C_K$ represent, respectively, the traveling time of ocean Rossby waves from the central to western IO and of ocean Kelvin waves across the basin; and C_R and C_K denote the speed of equatorial oceanic Rossby and Kelvin waves. Parameter C_0 represents the strength of the thermocline depth response to the wind forcing.

For simplicity, the thermocline depth anomaly in the western Pacific depends solely on the zonal wind anomaly in the central Pacific, that is,

$$\eta_{\mathrm{WP}} = -\frac{L_P\alpha U_{\mathrm{CP}}}{2\rho g' H}, \quad (4c)$$

where L_P is the half-width of the equatorial Pacific basin.

The anomalous monsoon heating over South Asia depends on both local and remote processes. For the local processes, the heating anomaly is determined by anomalous moisture convergence in the atmospheric boundary layer (CL00, Li et al. 2001b), which can be parameterized as

$$Q_I^{(1)} = \delta_I b\rho_a\Delta z L(\nabla\cdot\overline{\mathbf{V}}q)_I = \delta_I\sigma T_{\mathrm{WI}}, \quad (5a)$$

where subscript I denotes the Indian monsoon; δ_I represents the seasonality of the monsoon heating with $\delta_I = 1$ for June–July–August (JJA) and $\delta_I = 0$ otherwise, $b = 0.9$ is a fraction of the moisture convergence that condenses out and releases the latent heat following Kuo (1974), $\Delta z = 1500$ m denotes the depth of the atmospheric planetary boundary layer, and $q = (0.972T - 8.92) \times 10^{-3}$ is the surface air specific humidity, which is a function of SST (T) according to an empirical analysis by Li and Wang (1994).

Observations show that a dry Indian monsoon is often associated with an El Niño condition in the Pacific (Webster et al. 1998). To mimic this remote ENSO forcing, we parameterize the anomalous monsoon heating to be oppositely proportional to the eastern Pacific SSTA. Thus, the total anomalous heating may be written as

$$Q_I = \delta_I\sigma(T_{\mathrm{WI}} - c_1 T_{\mathrm{EP}}), \quad (5b)$$

where c_1 is a parameter representing the relative role of the local and remote SSTA forcing on the Indian monsoon. Note that the monsoon rainfall is slightly above normal in summer 1997, even though a strong El Niño developed in the Pacific. This abnormal monsoon–ENSO relationship is possibly attributed to the effect of the local SSTA as a strong dipole developed over the IO. While El Niño tends to suppress the monsoon, the IODM tends to enhance it and offset the El Niño effect. Given that the observed ratio of the SSTA between the western IO and eastern Pacific is 1:3 in summer 1997, $c_1 < 0.33$ implies that the local SSTA effect exceeds that of the remote ENSO forcing.

The anomalous monsoon may further feed back to the ocean by inducing cross-equatorial winds off the coast of Africa;

$$V_{\mathrm{WI}} = c_2' Q_I = \delta_I c_2(T_{\mathrm{WI}} - c_1 T_{\mathrm{EP}}). \quad (6a)$$

In addition to its effect on the monsoon, the El Niño may exert a strong impact on convection over the maritime continent. The suppression of convection in the maritime continent may further lead to anomalous southeasterly flows off Sumatra (as an atmospheric Rossby wave response to a heat sink). Combining both the ENSO forcing and the TAS feedback in the southeast IO, one may express the along-coastal wind anomaly off Sumatra as

$$V_{\mathrm{EI}} = c_3 T_{\mathrm{EP}} - c_4 T_{\mathrm{EI}}. \quad (6b)$$

The zonal wind anomaly over the central IO depends on 1) the east–west SSTA gradients (Lindzen and Nigam 1987), 2) the anomalous monsoon heating (CL00), and 3) the intensity of the local Walker cell controlled by the SSTA in the Maritime Continent (CL00):

$$U_I = \frac{A}{\varepsilon L_I}(T_{\mathrm{EI}} - T_{\mathrm{WI}}) + \delta_I c_5(T_{\mathrm{WI}} - c_1 T_{\mathrm{EP}}) + c_6 T_{\mathrm{WP}} + \tilde{f}(t), \quad (7a)$$

where A is an SST gradient momentum forcing coefficient (Wang and Li 1993), and ε is an atmospheric Rayleigh friction coefficient. The fourth term in the right-hand side of Eq. (7a) represents the atmospheric ISO forcing over the central equatorial IO. The inclusion of this term is to examine the role of the ISO on the initiation of the IODM.

The zonal wind anomaly in the western Pacific is determined by the anomalous monsoon heating that, by altering the planetary-scale east–west circulation, changes the surface wind in the western Pacific/Maritime Continent (Barnett et al. 1989; Meehl 1997; CL00):

$$U_{\mathrm{WP}} = -\delta_{\mathrm{I}} c_5 (T_{\mathrm{WI}} - c_1 T_{\mathrm{EP}}). \tag{7b}$$

The anomalous zonal wind in the central equatorial Pacific is simply determined by the east–west SST gradient:

$$U_{\mathrm{CP}} = \frac{A}{\varepsilon L_P}(T_{\mathrm{EP}} - T_{\mathrm{WP}}). \tag{7c}$$

It is worth mentioning that convective heating is a primary mechanism that drives the wind in the Tropics, while the SST gradient effect is relatively weak (Wang and Li 1993, Chiang et al. 2001). On the other hand, Lindzen and Nigam (1987) demonstrated that the SST gradient alone could force a realistic wind response if an unrealistically large boundary layer depth (say, 3 km) is used. Given the mathematical similarity of the two models (Neelin 1989), the use of the unrealistically large boundary layer depth may be regarded as a crude parameterization of inclusion of the convective heating effect.

The wind anomalies in turn drive ocean surface currents and vertical overturning. A simple 1.5-layer Cane–Zebiak (Cane 1979, Zebiak and Cane 1987) model is adopted to calculate the ocean surface current velocity and the Ekman pumping velocity:

$$u_I = \frac{\alpha U_I}{\rho h r}, \tag{8}$$

$$w_{\mathrm{WI}} = -\frac{2(H - h)u_I}{L_I}, \tag{9}$$

$$w_{\mathrm{EI}} = \frac{2(H - h)u_I}{L_I}, \tag{10}$$

$$u_{\mathrm{CP}} = \frac{\alpha U_{\mathrm{CP}}}{\rho h r}, \tag{11}$$

$$w_{\mathrm{WP}} = -\frac{(H - h)\beta\alpha U_{\mathrm{WP}}}{\rho H r^2} + \frac{2(H - h)u_{\mathrm{CP}}}{L_P}. \tag{12}$$

Here, β denotes the planetary vorticity gradient, H is the mean depth of the ocean thermocline, and r is a friction coefficient in the oceanic Ekman layer. Table 1 lists standard parameter values. Note that interactive coefficients $c_0, c_1, \ldots, c_6$ are determined by either regression from observational data or a scale analysis similar to that in CL00. For instance, we set $c_0 = 5$ s based on the observed sea level height–wind relationship that a 30-m height anomaly corresponds to a zonal wind anomaly of 6 m s^{-1} (see Fig. 4 of Webster et al. 1999); $c_6 = 4$ m s^{-1} k^{-1} implies that a half-degree SSTA in the Maritime Continent may lead to a zonal wind anomaly of 2 m s^{-1} in the central equatorial IO, which was derived from a scale analysis (see CL00 in detail) and supported by observations.

TABLE 1. List of standard model parameter values.

ρ_a	1.2 kg m^{-3}	$\overline{T}_0^{(x)}$	4×10^{-7} K m^{-1}
c_D	1.5×10^{-3}	$\overline{u}_0$	0.1 m s^{-1}
V_o	5 m s^{-1}	$\overline{V}_0$	4 m s^{-1}
h	50 m	$\overline{U}_{\mathrm{WP}}$ northern summer	2 m s^{-1}
H	150 m	$\overline{U}_{\mathrm{WP}}$ northern winter	-2 m s^{-1}
$g' = \frac{c_K^2}{H}$	$\frac{2.5^2}{150}$ m s^{-2}	$\overline{T}_{\mathrm{WI}}^{(z)}$, $\overline{T}_{\mathrm{EI}}^{(z)}$	0.02 K m^{-1}
A	50 m^2 s^{-2} K^{-1}	$\overline{T}_{\mathrm{WP}}^{(z)}$	0.01 K m^{-1}
ε	10^{-5} s^{-1}	$\overline{w}_0$	4×10^{-6} m s^{-1}
L_I	4×10^6 m	$\overline{w}_c$	10^{-6} m s^{-1}
L_P	8×10^6 m	$\Delta\overline{q}_{\mathrm{WI}}$, $\Delta\overline{q}_{\mathrm{EI}}$, $\Delta\overline{q}_{\mathrm{WP}}$	5×10^{-3}
γ	0.1 K m^{-1}	r	10^{-5} s^{-1}
κ	7×10^{-4} K^{-1}	c_0	5 s
c_1	0.25	c_2	1 m s^{-1} K^{-1}
c_3	0.5 m s^{-1} K^{-1}	c_4	1 m s^{-1} K^{-1}
c_5	2 m s^{-1} K^{-1}	c_6	4 m s^{-1} K^{-1}

b. Basic state, model physics, and external forcing

The basic-state winds along the coasts of Sumatra and Somalia exhibit a strong annual cycle. In response to this wind forcing, the coastal upwelling also exhibits a clear annual variation, with maximum amplitude appearing in boreal summer. To mimic this observed feature, we specify the basic-state wind and the vertical velocity at the base of the ocean mixed layer as follows:

$$\overline{V}_{\mathrm{WI}} = \overline{V}_{\mathrm{EI}} = \overline{V}_0 \cos\left[\frac{2\pi(i - 7)}{12}\right], \tag{13}$$

$$\overline{w}_{\mathrm{WI}} = \overline{w}_{\mathrm{EI}} = \max\left\{\overline{w}_C, \overline{w}_0 \cos\left[\frac{2\pi(i - 7)}{12}\right]\right\}, \tag{14}$$

where $i = 1, 2, \ldots, 12$ represents January, February, . . . , December; and $\overline{w}_C$ is a minimum vertical velocity representing vertical mixing due to the background wind stirring. Same as in CL00, a seasonally varying basic-state zonal wind is specified over the Maritime Continent.

The basic-state zonal wind and east–west SST gradient exhibit a semiannual cycle in the equatorial central IO (Ueda 2001). To mimic this observational feature, we specify the following basic-state ocean current and zonal temperature gradient in the central IO:

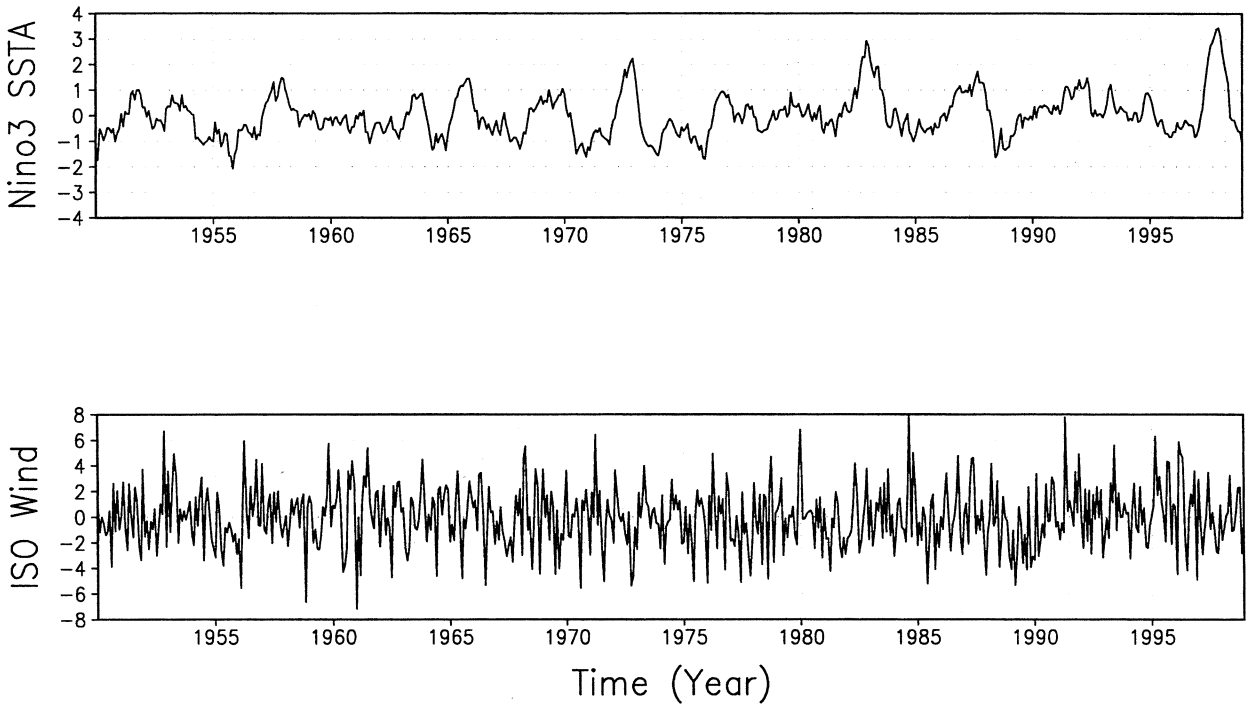

FIG. 7. Time series of the external ENSO and ISO forcing specified in the model. (top) The observed Niño-3 SSTA (°C) during 1950–99. (bottom) The 10–90-day filtered zonal wind (m s^{-1}) in the central equatorial Indian Ocean (60°–90°E, 5°S–5°N).

$$\overline{u}_I = \overline{u}_0 \cos\left[\frac{2\pi(i-4)}{6}\right], \tag{15}$$

$$\overline{T}_I^{(x)} = -\overline{T}_0^{(x)} \cos\left[\frac{2\pi(i-4)}{6}\right]. \tag{16}$$

Various positive and negative air–sea feedback processes are involved in the model. The negative feedback processes include the cloud–radiation–SST feedback, the wind–evaporation–SST feedback, and the monsoon–ocean feedback. The positive feedback processes include the thermocline–SST–wind feedback and the TAS feedback. Ocean waves have a positive (negative) impact on the initial (late) development stage of the IODM.

In addition to internal ocean–atmosphere interactions in the IO, the model is subjected to two types of external forcings, the ISO and ENSO. It has been long noticed that the tropical IO is a region with strong intraseasonal variability. It is not clear, however, what role the ISO plays in the dipole mode development. As the greatest interannual variability in the Tropics, ENSO may exert a strong impact on the IO. A key question is how the El Niño impacts the IO SST. We hypothesize that the El Niño may influence the IO through the following three processes: 1) cooling of the SSTA in the western Pacific/Maritime Continent, which further alters the strength of the local Walker cell over the IO; 2) decrease of intensity of the South Asian monsoon through large-scale east–west circulation, which further reduces the strength of the Somalia Jet and the monsoon westerly over the equatorial central IO; and 3) suppression of convection in the Maritime Continent that may further induce anomalous southeasterly off Sumatra as a direct response of atmospheric Rossby waves to the heat sink. To realistically describe the forcing strength, observed time series of the 10–90-day filtered zonal wind field in the central equatorial IO and the Niño-3 SSTA during 1950–98 were specified for $\tilde{f}(t)$ and $T_{\rm EP}$ in the model (see Fig. 7).

4. The model solutions in the absence of external forcing

First we examine the model solutions in the absence of any external forcings [$\tilde{f}(t) = T_{\rm EP} = 0$]. The purpose of this experiment is to examine whether or not ocean–atmosphere interactions alone in the warm oceans can support a self-sustained oscillation. Initially, an idealized dipole SST structure, with $T_{\rm WI} = 0.5$°C and $T_{\rm EI} = -0.5$°C, was specified. Figure 8a shows the time evolution of the model SSTA in this case. The result indicates that the IODM is a dynamically coupled air–sea mode whose instability depends strongly on season. In general, the atmosphere–ocean interactions in the warm oceans tend to enhance the dipole mode in northern summer but dampen it in northern winter. As a result, the IODM has a distinctive evolution characteristic compared to the El Niño. Overall, our simple model results suggest that the IODM be a weakly damped oscillator, with a biennial periodicity, in the absence of external forcing.

Diagnosis of the surface heat budget indicates that

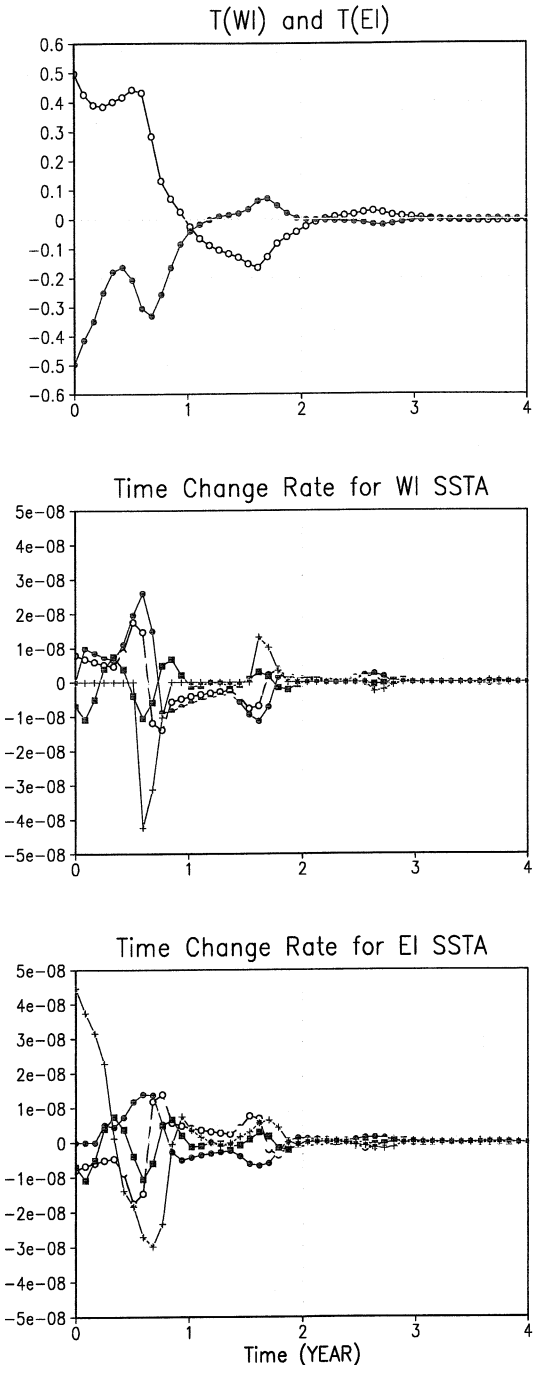

FIG. 8. Evolution of simulated SSTA (°C) in the western (open circle) and eastern (closed circle) Indian Ocean in the absence of (top) external forcing and time tendencies of the SSTA (°C s^{-1}) in the (middle) western and (bottom) eastern IO. In the middle and bottom, the open and closed circles denote anomalous vertical temperature advection associated with fast thermocline adjustments and slower oceanic wave effects. The open square represents the vertical temperature advection due to anomalous upwelling. The closed square represents the horizontal temperature advection anomaly. The cross denotes the evaporation–SST–wind feedback associated with the anomalous monsoon for the western IO and the TAS feedback for the eastern IO.

TABLE 2. Sensitivity of growth rates (yr^{-1}) to the change of model key parameters from 50% to 150% of their standard values.

	50%	100%	150%
c_0	−1.5	−1.4	−1.2
c_2	−1.6	−1.4	−1.3
c_4	−1.3	−1.4	−1.4
c_5	−2.9	−1.4	−0.5
c_6	−2.3	−1.4	−0.8

the time change rate of T_{WI} is primarily determined by anomalous vertical temperature advection (including the effect of ocean waves) and evaporational cooling associated with the monsoon–ocean local feedback (Fig. 8b). The time change rate of T_{EI} is strongly regulated by the seasonal-dependent TAS feedback (Fig. 8c). The anomalous vertical temperature advection tends to enhance T_{EI} in the initial development stage due to the positive thermocline–SST feedback, but tends to decrease T_{EI} later owing to the delayed effect of the ocean waves. In both regions, the cloud–radiation–SST feedback contributes greatly to damping the SSTA, while the zonal advection anomaly has modest amplitude with a semiannual periodicity.

Given that the simple model contains a number of tunable parameters, it is necessary to test the sensitivity of the model solution to key parameters. Table 2 shows results from 15 sensitivity experiments in which several key model parameters have been increased or decreased by 50% of their standard values. The growth rates in Table 2 were calculated based on the time series of the west–east SSTA difference, taking into account both oscillating and decaying components. The growth rates in Table 2 all point a negative sign, indicating that the solution that the IODM is a weakly damped oscillator is robust.

Physically, it is argued that El Niño can be self-sustained because of the shallow mean thermocline in the eastern Pacific that permits a strong positive dynamic air–sea feedback and because of the cloud–SST phase difference that minimizes a potentially strong negative thermodynamic feedback. This is distinctive from that in the equatorial IO where the mean thermocline is much deeper and where there is a strong negative cloud-SST feedback. The greatest negative feedback in the IO comes from the cloud–radiation–SST feedback. Additional negative feedback results from the monsoon–ocean interaction.

The notion that the IODM is not self-sustained in the absence of external forcing does not imply that the SST perturbation cannot grow in all time. In fact, our results show that during boreal summer the TAS positive feedback may overcome the sum of the negative feedbacks; as a result, perturbations triggered prior to summer may continue to grow through summer and reach a mature phase in fall. This seasonal-dependent coupled instability is crucial for the phase-locking feature of the IODM, which will be discussed in section 6.

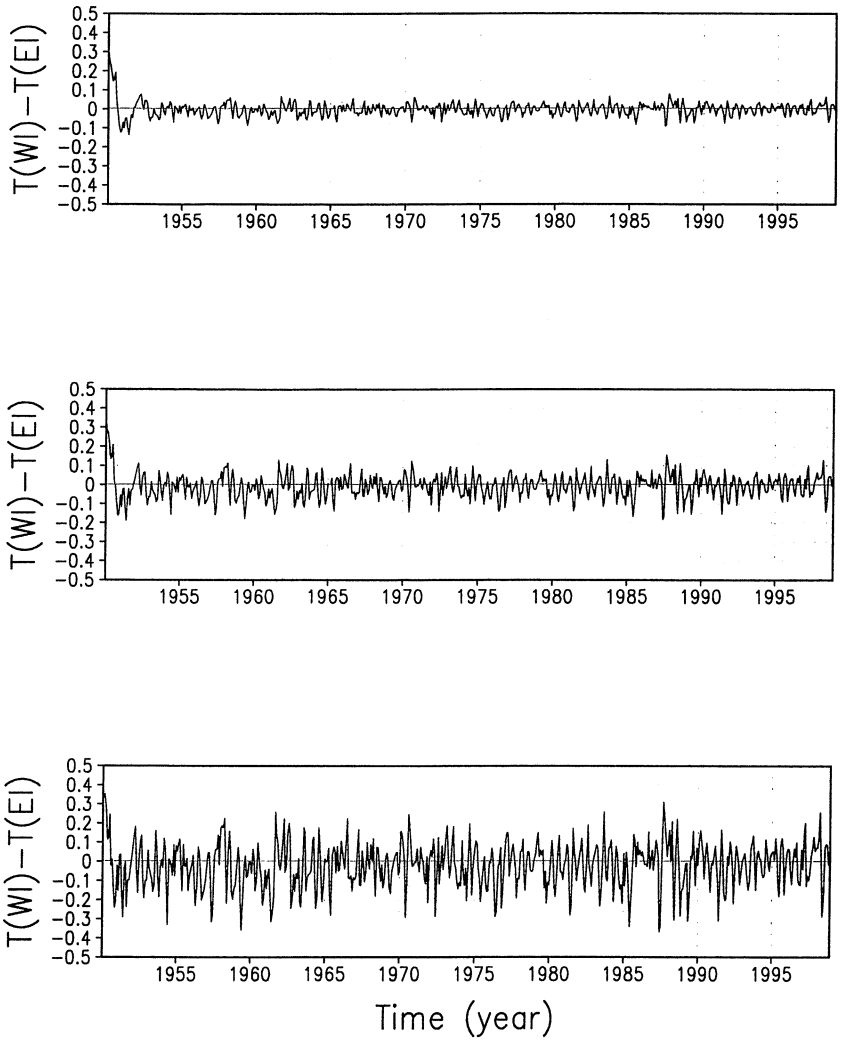

FIG. 9. Evolution of the SSTA difference (°C) between the western and eastern IO in the presence of (top) a quarter, (middle) a half, and (bottom) full strength of the observed ISO wind forcing in the central equatorial IO. All other parameters are same as those in Fig. 8.

5. Role of external forcing

To examine the impact of the ISO, we designed a set of numerical experiments in which the strength of the ISO was gradually increased to the 25%, 50%, and 100% of the observed amplitude. Figure 9 shows the simulated SSTA evolution in the three cases. With enhanced ISO variability, the IODM tends to oscillate around a finite amplitude, suggesting that the ISO may act as stochastic forcing to reinvigorate the natural damped mode. However, even with the full strength of the ISO forcing, the amplitude of the SSTA is still much weaker compared to the observed IO SSTA variability.

In the presence of the realistic El Niño forcing, the model is capable of simulating several major IODM events (i.e., in 1997, 1982, and 1963) during last 50 yr. Figure 10 shows the model simulated SSTA in the western and eastern IO, along with observed counterparts. The results indicate that ENSO is one of major forcing mechanisms that trigger the IODM events.

In the model, the El Niño influences the IODM mainly through the change of intensity of the Indian monsoon and of convection over the maritime continent. To investigate their relative roles, two additional experiments were conducted in which we isolated each of the two processes ($c_1 = 0$ versus $c_3 = 0$). The results show that both processes contribute nearly equally to the development of the IODM (figure not shown).

The failure of simulation of the 1961 and 1994 events implies that other types of climate forcings must play a role in initiating an IODM event. A recent coupled model study by Lau and Nath (2003b, manuscript submitted to *J. Climate*) pointed out that one such triggering mechanism is a zonally elongated sea level pressure anomaly situated south of Australia in association with the Antarctic annual mode in southern winter.

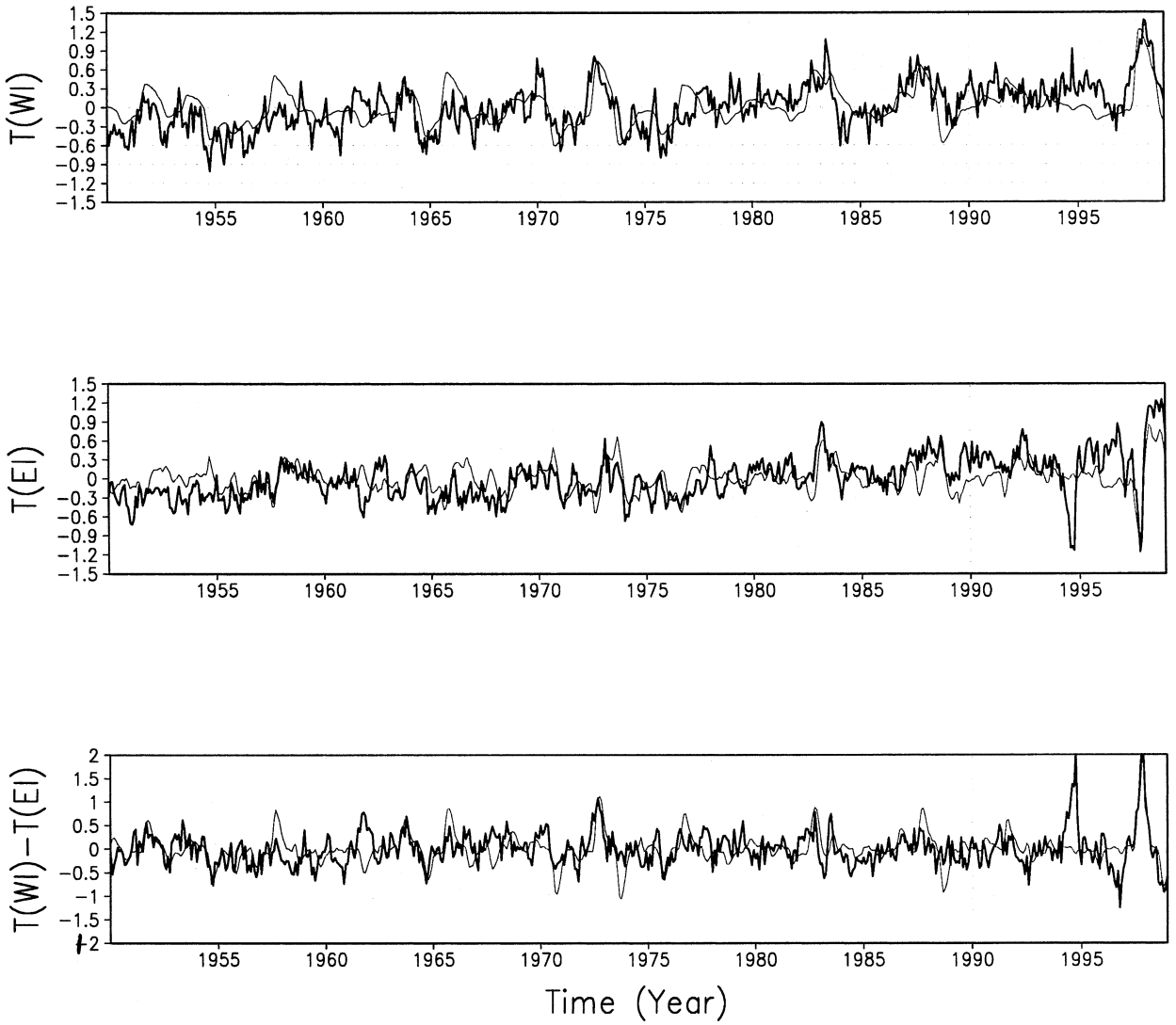

FIG. 10. Evolution of observed (thick line) and simulated (thin line) SST anomalies (°C) in the (top) western and (middle) eastern Indian Ocean and (bottom) their differences. Observed El Niño and ISO forcing was specified in this case, and all other parameters have the same values as those in Fig. 8.

6. Phase-locking mechanism

Although the El Niño has a remote impact on the wind in the IO, it is the local ocean–atmosphere interactions and the annual cycle of the basic state that regulate the IODM evolution. This is why the peak phase of the IODM occurs in October even though the El Niño forcing peaks in northern winter. Various basic-state factors may contribute to the phase locking of the IODM. The first is the annual cycle of the basic-state wind off Sumatra. This seasonally varying wind may regulate the local SST change through the TAS feedback mechanism. The second is the seasonal change of the basic-state upwelling off the coasts of Sumatra and Somalia. It may give rise to a greater SST tendency in boreal summer when the upwelling is stronger. The third is the annual cycle of the zonal SST gradient and zonal wind at the equator. Ueda (2001) argued that this basic-state factor may give rise to a peak phase of the IODM in northern fall. The fourth factor is the seasonal dependence of the monsoon heating. Although the El Niño has the greatest amplitude toward the end of a year, its impact on the monsoon peaks in northern summer. Thus, the El Niño may have a maximum indirect effect (through the monsoon) on the IODM after summer.

Figure 11 shows the composite evolution of the dipole mode index (SSTA difference between the western and eastern IO) and the IO zonal wind anomaly in a control case when all aforementioned factors are considered. The composite is based on seven strongest IODM events derived from the time series of Fig. 10. Note that the peak IODM phase occurs in October, similar to the observed. The conceptual model is able to simulate the phase-locking feature of the IODM.

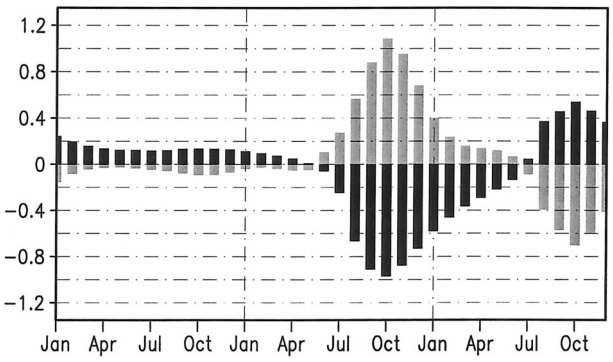

FIG. 11. Evolution of the model composite SSTA difference (°C, light-shaded bar) and zonal wind anomaly (2 m s^{-1}, dark-shaded bar) in the Indian Ocean.

To investigate the relative roles of the aforementioned factors, we designed the following four experiments. In the first experiment we took into account the effect of the annual cycle of $\overline{V}_{\mathrm{EI}}$ while keeping the annual mean value for other basic-state variables. In the second experiment we considered the seasonally varying $\overline{w}_{\mathrm{EI}}$ and $\overline{w}_{\mathrm{WI}}$ only. In the third experiment the effect of annual cycle of $\overline{u}_I$ and $\overline{T}_I^{(x)}$ was examined. In the fourth experiment we considered the seasonally varying $\overline{V}_{\mathrm{WI}}$ and $\overline{U}_{\mathrm{WP}}$.

Figure 12 illustrates the results from the four experiments. While their time series look similar, the major difference lies in the timing of their peak phases. The mature phase of the IODM appears in October for experiments 1 and 4 but in January for experiments 2 and 3. The results indicate that the primary mechanisms for the phase locking arise from the seasonal-dependent TAS feedback (Fig. 12a) and the indirect El Niño effect on the IO (through the anomalous monsoon) (Fig. 12d). The effect of the seasonal varying upwelling and zonal temperature gradient is of secondary importance (Figs. 12b,c).

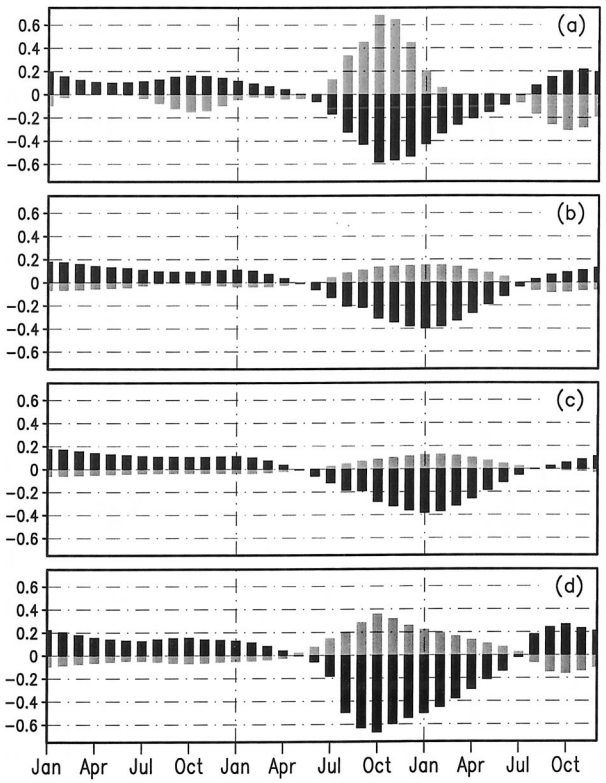

FIG. 12. Same as Fig. 11, except for specification of different annual cycle basic states. (a) A case when only the annual cycle of the wind over the eastern IO is included. (b) A case in which only the annual cycle of ocean upwelling along the coasts of Africa and Sumatra is considered. (c) A case of annually varying zonal oceanic currents and zonal temperature gradients. (d) A case that considers the annual cycle of the wind in both the western IO and the Maritime Continent.

7. Effect of ocean waves

Observations show that the IODM developed rapidly in summer 1997 and reached its peak phase in fall. After that, the cold SSTA in the eastern IO started to decay, while the warm SSTA in the western IO spread into the east. By the end of winter 1997/98, a basinwide warming (hereafter, referred to as a unimode) was observed.

Such a dipole-to-unimode transition is well captured by the model. Figure 13a illustrates the evolution of the simulated SSTA in 1997, along with observed counterparts. Similar to the observations, after the cold SSTA in the eastern IO reached its maximum amplitude in October, it decayed rapidly and became positive in December 1997. What causes such a dipole-to-unimode transition? The diagnosis of the SSTA budget showed that the primary mechanism for this SSTA transition was attributed to the delayed effect of the reflected oceanic Kelvin waves. As discussed in section 2, westward-propagating oceanic Rossby waves were excited by the curl of the wind stress anomalies in the central equatorial IO. After reflected from the western boundary, the Rossby waves became downwelling equatorial Kelvin waves that propagated eastward. The eastward expansion of the warm SSTA was attributed to the accumulated effect of the Kelvin waves. When the wave effect is excluded (by setting $c_0 = 0$), the SSTA transition does not occur (see Fig. 13b). The effect of ocean waves and associated thermocline changes on the eastern IO SSTA transition is supported by recent observational studies (Ansell 2002; Feng and Meyers 2003).

In addition to the ocean wave effect, the anomalous latent heat flux may also contribute to the SSTA transition off Sumatra (see Fig. 3 of Li et al. 2002). This effect, however, is underestimated in the current model due to the lack of the zonal wind anomaly over the eastern IO box.

8. Biennial tendency of the IODM

The composite model SST and wind evolution (see Fig. 11) shows a biennial tendency, similar to the ob-

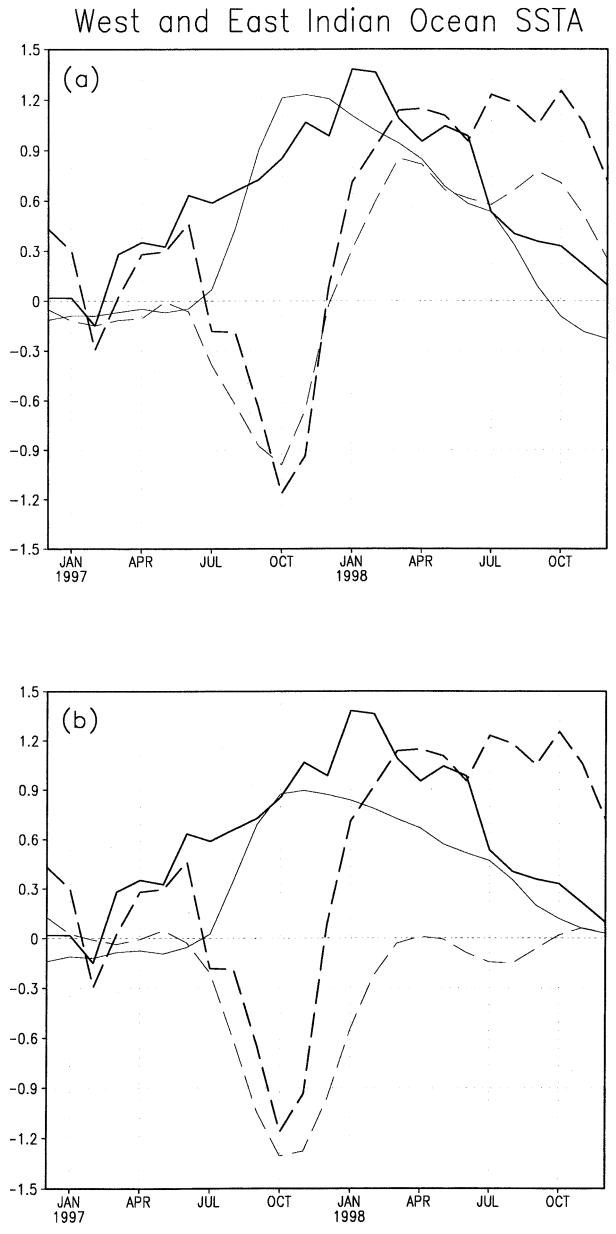

FIG. 13. Evolution of the observed (thick line) and simulated (thin line) SSTA (°C) in the western (solid line) and eastern (dashed line) IO associated with the 1997/98 IODM event. (top) The case that includes the effect of oceanic waves, and (bottom) a case without the oceanic wave effect.

served. What cause this biennial tendency? One obvious factor is the El Niño forcing, which has a quasi-biennial component. Another possible factor is the monsoon–ocean interaction that may lead to a biennial oscillation in the monsoon region (CL00; Li et al. 2001a). To illustrate the role of the monsoon–ocean interaction, we conducted an experiment in which all parameters were set the same as those in Fig. 8, except that we turned off the effect of the monsoon (by setting $Q_I = 0$). The result clearly illustrates the importance of the monsoon–ocean interaction in causing the biennial tendency of the IODM. Contrary to Fig. 8a in which the SSTA in the IO alters its sign from one year to the following year, the SSTA in the case of no monsoon feedback does not cross the zero line (see Fig. 14).

How does the monsoon–ocean feedback lead to a biennial tendency? As we know, a positive phase of the IODM may lead to a strong Indian monsoon. The enhanced monsoon induces anomalous east–west circulation, leading to a positive tendency of the SSTA in the Maritime Continent (CL00). The anomalous warming in the Maritime Continent further exerts a delayed impact on the equatorial IO through the enhanced local Walker cell, leading to the development of a negative phase of the IODM in the following year. Thus, it is the lagged response of the maritime continent SSTA to the anomalous monsoon that gives rise to the biennial tendency of the IODM.

9. Conclusions and discussions

In this study we investigate the origin of the Indian Ocean dipole–zonal mode (IODM) based on observational analyses and a conceptual coupled atmosphere–ocean model. We addressed the following scientific questions. What are fundamental differences of air–sea interactions between the tropical Pacific and Indian Oceans? Why does the peak phase of the IODM appear in October? What are mechanisms responsible for the biennial tendency of the IODM? Is the IODM a self-sustained coupled mode? What roles do the ENSO and ISO play in the IODM evolution?

Four fundamental differences of air–sea coupling processes between the tropical Pacific and Indian Oceans are identified. The first difference is represented by the contrast of the cloud–SST phase relationship between the warm pool and cool tongue. The in-phase cloud–SST relationship in the IO leads to a strong negative feedback, while a significant phase difference in the El Niño scenario leads to a much weaker thermodynamic damping. The second difference arises from the reversal of the basic-state zonal wind and the tilting of the ocean thermocline, which leads to distinctive effects of ocean waves on the SST, especially in the initial development stage of the IODM. The third difference lies in the monsoon–ocean interaction. A positive phase of the IODM tends to enhance the South Asian monsoon, whereas the strengthened monsoon tends to damp the IODM. The fourth difference is that the southeast Indian Ocean is a region where a positive thermodynamic air–sea feedback exists between an anomalous atmospheric anticyclone and a cold SSTA in northern summer.

A conceptual coupled atmosphere–ocean model was constructed based on the observational analyses and physical reasoning. This model contained five boxes that represent the equatorial western and eastern Indian Ocean, the western Pacific/Maritime Continent, the equatorial eastern Pacific, and the South Asian monsoon

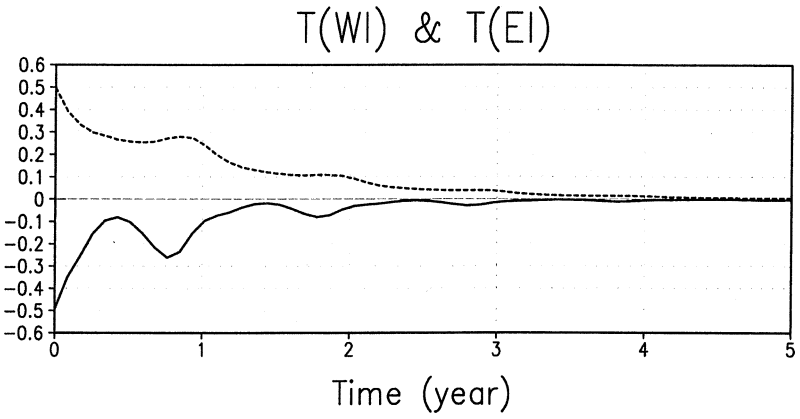

FIG. 14. Evolution of the SSTA (°C) in the western (dashed line) and eastern (solid line) IO in the absence of the monsoon feedback. All other parameters are same as those in the case shown in Fig. 8.

region, respectively. In the model, various positive and negative air–sea feedback processes are considered. Among them are the cloud–radiation–SST feedback, evaporation–wind feedback, thermocline–SST feedback, and the monsoon–ocean feedback. Our results indicate that the IODM is a dynamically coupled atmosphere–ocean mode whose instability depends on season. The air–sea interaction in the warm oceans in general tends to enhance the dipole mode in boreal summer but dampens it in boreal winter. Overall, the simple model results suggest that the IODM be a weakly damped oscillator in the absence of external forcing, which differs from the self-sustained ENSO mode in the Pacific. The essential cause for such a difference arises from much deeper mean thermocline in the equatorial IO that prevents an efficient dynamic air–sea coupling and a strong thermodynamic damping resulting from the negative cloud–SST feedback.

Contrary to the southeast tropical Pacific and Atlantic Oceans characterized by cold SST tongues and dense low-level stratus clouds, the southeast IO (off Sumatra) is a region with high mean SST and deep convection. Because of this distinctive feature, a positive thermodynamic air–sea feedback arises from the interaction between an anomalous atmospheric anticyclone and a cold SSTA. This TAS feedback mechanism is season dependent due to its dependence on the basic-state wind. A positive feedback occurs in boreal summer when the southeasterly flow is pronounced. It becomes a negative feedback in northern winter. The phase locking of the IODM can be, to a large extent, explained by this seasonal-dependent TAS feedback mechanism. In addition, the monsoon also plays a role. Although the El Niño matures in December, its impact on the monsoon peaks in northern summer. Therefore, the El Niño may have a maximum indirect impact on the IO SSTA after summer.

The fact that the IODM peaks in northern fall, by which time the Indian monsoon has all but ended, does not contradict the negative monsoon–IODM feedback. This is because, even though the monsoon tends to feedback negatively to the IODM, the positive TAS feedback overcomes its negative effect. As a result, the IODM continues to grow in boreal summer and reaches a mature phase in northern fall.

Unlike the equatorial Pacific, where thermocline is tilted to the east, the thermocline in the equatorial IO is shallower toward the west. As a result, except a few hundred of kilometers off the coast of Sumatra, the SST is more sensitive to the thermocline change in the west than in the east. Thus, ocean waves tend to have a positive impact on the IODM during its initial development stage. The reflected Kelvin waves also have a negative effect on the SSTA in the eastern IO, but this effect is overwhelmed by the positive TAS feedback in summer. Thus, the negative wave effect is realized only in the late development stage when it contributes to the dipole-to-unimode conversion.

The biennial tendency of the IODM arises partially from the remote impact of the monsoon on the Maritime Continent SSTA. This is because a positive phase of the IODM leads to an enhanced monsoon, and the strengthened monsoon further leads to a delayed response of the SSTA in the Maritime Continent. The local Walker cell induced by the delayed warm Maritime Continent SSTA may lead to a negative phase of the IODM in the following year. The El Niño also contributes to the biennial tendency due to its quasi-biennial component.

The role of the ISO was investigated by forcing the model with the observed ISO (10–90-day filtered) wind in the central equatorial IO. With the increase of strength of the ISO forcing, the model simulates a weak, irregular oscillation, suggesting that the ISO may act as a stochastic forcing to reinvigorate the naturally damped mode.

While the ISO primarily represents atmospheric stochastic forcing, the ENSO has a more profound impact on the IODM due to its long duration and great ampli-

tude. The El Niño impacts the IODM in the model through the following three processes. First, it influences the strength of the South Asian monsoon, which further alters the cross-equatorial wind along the coast of Africa and zonal wind in the central equatorial IO. Second, it altered the anomalous Walker cell over the IO through the change of SST in the Maritime Continent. Third, it influences the intensity of convection over the Maritime Continent, which further induces anomalous along-coastal winds off Sumatra (as a direct Rossby wave response to an anomalous heat source). The three processes all favor the initiation of a positive phase of the IODM. In the presence of realistic ENSO forcing, the model was capable of simulating most IODM events during recent 50 yr that were associated with the ENSO, indicating that ENSO is one of major triggering mechanisms. The failure of simulation of the IODM events in 1961 and 1994 suggests the possibility of other types of climate forcings in triggering a dipole event.

The search for triggering mechanisms for the 1961 and 1994 events is currently under investigation. Given that the conceptual model contains a number of tunable parameters and simplified physics, caution is needed in interpreting the damped oscillator result. It is desirable to extend the current scope by using a sophisticated coupled atmosphere–ocean GCM.

Acknowledgments. We thank Gabriel Lau and anonymous reviewers for their valuable suggestions. This work was supported by the NOAA Grant NA01AANRG0011 and NSF Grant ATM01-19490. International Pacific Research Center is partially sponsored by the Frontier Research System for Global Change.

REFERENCES

Ansell, T., 2002: Air–sea interaction in the tropical Indian Ocean and links with Australian rainfall variability. Ph.D. thesis, School of Earth Science, University of Melbourne, 272 pp.

Ashok, K., Z. Guan, and T. Yamagata, 2001: Impact of the Indian Ocean dipole on the relationship between the Indian monsoon rainfall and ENSO. *Geophys. Res. Lett.,* **28,** 4499–4502.

Barnett, T. P., L. Dumenil, U. Schlese, E. Roeckner, and M. Latif, 1989: The effect of Eurasian snow cover on regional and global climate variations. *J. Atmos. Sci.,* **46,** 661–685.

Battisti, D. S., and A. C. Hirst, 1989: Interannual variability in the tropical atmosphere–ocean system: Influence of the basic state and ocean geometry. *J. Atmos. Sci.,* **46,** 1678–1712.

Cane, M. A., 1979: The response of an equatorial ocean to simple wind stress patterns. I: Model formulation and analytic results. *J. Mar. Res.,* **37,** 233–252.

Chambers, D. P., B. D. Tapley, and R. H. Stewart, 1999: Anomalous warming in the Indian Ocean coincident with El Niño. *J. Geophys. Res.,* **104,** 10 523–10 533.

Chang, C.-P., and T. Li, 2000: A theory for the tropical tropospheric biennial oscillation. *J. Atmos. Sci.,* **57,** 2209–2224.

Chiang, J. C. H., S. Z. Zebiak, and M. A. Cane, 2001: Relative roles of elevated heating and surface temperature gradients in driving anomalous surface winds over the tropical oceans. *J. Atmos. Sci.,* **58,** 1371–1394.

Feng, M., and G. Meyers, 2003: Interannual variability in the tropical Indian Ocean: A two-year time scale of the Indian Ocean dipole. *Deep-Sea Res.,* in press.

Gill, A. E., 1980: Some simple solutions for heat-induced tropical circulation. *Quart. J. Roy. Meteor. Soc.,* **106,** 447–462.

Hackert, E., and S. Hastenrath, 1986: Mechanics of Java rainfall anomalies. *Mon. Wea. Rev.,* **114,** 745–757.

Kuo, H.-L., 1974: Further studies of the parameterization of the influence of cumulus convection on large-scale flow. *J. Atmos. Sci.,* **31,** 1231–1240.

Lau, N.-C., and M. J. Nath, 2003a: Atmosphere–ocean variations in the Indo-Pacific sector during ENSO episodes. *J. Climate,* **16,** 3–20.

Li, T., 1997: Phase transition of the El Niño–Southern Oscillation: A stationary SST mode. *J. Atmos. Sci.,* **54,** 2872–2887.

——, and B. Wang, 1994: A thermodynamic equilibrium climate model for monthly mean surface winds and precipitation over the tropical Pacific. *J. Atmos. Sci.,* **51,** 1372–1385.

——, C.-W. Tham, and C.-P. Chang, 2001a: A coupled air–sea–monsoon oscillator for the tropospheric biennial oscillation. *J. Climate,* **14,** 752–764.

——, Y. S. Zhang, C. P. Chang, and B. Wang, 2001b: On the relationship between Indian Ocean SST and Asian summer monsoon. *Geophys. Res. Lett.,* **28,** 2843–2846.

——, ——, E. Lu, and D. Wang, 2002: Relative role of dynamic and thermodynamic processes in the development of the Indian Ocean dipole. *Geophys. Res. Lett.,* **29,** 2110–2113.

Lindzen, R. S., and S. Nigam, 1987: On the role of sea surface temperature gradients in forcing low-level winds and convergence in the tropics. *J. Atmos. Sci.,* **44,** 2240–2458.

Meehl, G. A., 1997: The south Asian monsoon and the tropospheric biennial oscillation. *J. Climate,* **10,** 1921–1943.

Murtugudde, R., J. P. McCreary Jr., A. J. Busalacchi, 2000: Oceanic processes associated with anomalous events in the Indian Ocean with relevance to 1997–1998. *J. Geophys. Res.,* **105,** 3295–3306.

Neelin, J. D., 1989: On the interpretation of the Gill model. *J. Atmos. Sci.,* **46,** 2466–2468.

——, 1991: The slow sea surface temperature mode and the fast wave limit: Analytical theory for tropical interannual oscillation and experiments in a hybrid coupled model. *J. Atmos. Sci.,* **48,** 584–606.

Reverdin, G., D. L. Cadet, and D. Gutzler, 1986: Interannual displacement of convection and surface circulation over the equatorial Indian Ocean. *Quart. J. Roy. Meteor. Soc.,* **112,** 43–67.

Saji, N. H., B. N. Goswami, P. N. Vinayachandran, and T. Yamagata, 1999: A dipole mode in the tropical Indian Ocean. *Nature,* **401,** 360–363.

Schopf, P. S., and M. J. Suarez, 1988: Vacillations in a coupled ocean–atmosphere model. *J. Atmos. Sci.,* **45,** 549–566.

Ueda, H., 2001: Equatorial monsoon system as regulation for a dipole mode in the Indian Ocean. *Pap. Meteor. Geophys.,* **51,** 147–154.

——, and J. Matsumoto, 2000: A possible process of east–west asymmetric anomalies over the Indian Ocean in relation to 1997/98 El Niño. *J. Meteor. Soc. Japan,* **78,** 803–818.

Wang, B., and T. Li, 1993: A simple tropical atmospheric model of relevance to short-term climate variations. *J. Atmos. Sci.,* **50,** 260–284.

——, and X. Xie, 1998: Coupled modes of the warm pool climate system. Part I: The role of air–sea interaction in maintaining Madden–Julian Oscillation. *J. Climate,* **11,** 2116–2135.

——, R. Wu, and X. Fu, 2000: Pacific–East Asian teleconnection: How does ENSO affect East Asian climate? *J. Climate,* **13,** 1517–1536.

——, ——, and T. Li, 2003: Atmosphere–warm ocean interaction and its impact on Asian–Australian Monsoon variation. *J. Climate,* **16,** 1195–1211.

Webster, P. J., V. O. Magana, T. N. Palmer, J. Shukla, R. A. Tomas, M. Yanai, and T. Yasunari, 1998: Monsoons: Processes, pre-

dictability, and the prospects for prediction. *J. Geophys. Res.*, **103** (C7), 14 451–14 510.
——, A. M. Moore, J. P. Loschnigg, and R. R. Leben, 1999: Coupled ocean–atmosphere dynamics in the Indian Ocean during 1997–98. *Nature*, **401,** 356–360.
Xie, S.-P., H. Annamalai, F. A. Schott, and J. P. McCreary Jr., 2002: Structure and mechanisms of South Indian Ocean climate variability. *J. Climate*, **15,** 864–878.
Zebiak, S. E., and M. A. Cane, 1987: A model ENSO. *Mon. Wea. Rev.*, **115,** 2262–2278.